Planetary and Space Science 59 (2011) 1665–1669

Contents lists available at ScienceDirect

Planetary and Space Science

journal homepage: www.elsevier.com/locate/pss

Rapid Communication

Predictions of MESSENGER Neutron Spectrometer measurements for Mercury's north polar region

David J. Lawrence [a,*], John K. Harmon [b], William C. Feldman [c], John O. Goldsten [a], David A. Paige [d], Patrick N. Peplowski [a], Edgar A. Rhodes [a], Christina M. Selby [a], Sean C. Solomon [e]

[a] Johns Hopkins University Applied Physics Laboratory, Laurel, MD 20723, USA
[b] National Astronomy and Ionosphere Center, Arecibo Observatory, Arecibo, PR 00612, USA
[c] Planetary Science Institute, Tucson, AZ 85719, USA
[d] Department of Earth and Space Sciences, University of California, Los Angeles, CA 90095, USA
[e] Department of Terrestrial Magnetism, Carnegie Institution of Washington, Washington, DC 20015, USA

ARTICLE INFO

Article history:
Received 4 February 2011
Received in revised form
29 June 2011
Accepted 1 July 2011
Available online 6 July 2011

Keywords:
Mercury
Polar deposits
Neutron spectroscopy
MESSENGER

ABSTRACT

From radar images of Mercury's poles and MESSENGER Neutron Spectrometer (NS) measurements obtained during the spacecraft's flybys of Mercury, predictions of neutron count rates and their uncertainties are calculated for Mercury's north polar region as of the end of the MESSENGER primary orbital mission. If Mercury's poles contain large amounts of water ice, as has been suggested on the basis of the radar data, then during the one-year-long orbital mission the NS should detect signals indicative of excess polar hydrogen with a significance of at least 4σ, where σ is the standard deviation derived from Poisson counting statistics. If the polar deposits are not enriched with hydrogen, but are dominated by other elements, such as sulfur, then the MESSENGER neutron measurements should be able to confirm the absence of deposits having surface concentrations in excess of 50 wt% H_2O on permanently shadowed floors of craters near Mercury's north pole. Because of the large spatial footprint of the NS data, individual polar deposits will not be spatially resolved, but longitudinal asymmetries may be detected if residual systematic uncertainties are sufficiently low.

1. Introduction

Permanently shaded regions (PSRs) at the poles of planetary bodies are of great interest because of their special properties. The most well-studied PSRs are those of Mercury and the Moon. PSRs are present on those bodies because their axes of rotation are nearly perpendicular to their orbital planes, and impact craters near each pole are sufficiently deep to be continuously shaded from sunlight for geologically long periods of time. Because these planetary bodies have no atmosphere to transport heat from equatorial regions, PSRs reach very cold temperatures (Paige et al., 1992, 2010; Vasavada et al., 1999). At such low temperatures, volatiles from multiple sources (asteroidal and cometary impacts, micrometeoroid bombardment, solar wind implantation) can be trapped in the PSRs (Lucey, 2009). Thus, there were early predictions (Watson et al., 1961; Arnold, 1979) that PSRs could be enriched in volatile species such as water ice.

The discovery of Mercury's polar deposits by Earth-based radar and the suggestion that those deposits may consist dominantly of water ice enrichments were made two decades ago (Harmon and Slade, 1992; Slade et al., 1992). The radar signature of water ice is an enhancement of reflected same-sense polarized waves when the surface is illuminated at radio wavelengths. Subsequent Earth-based radar measurements by the Arecibo Observatory have led to marked improvements in our understanding of the location of the polar deposits and the possible distribution of water ice near Mercury's poles. From 5 years of Arecibo S-band (2380 MHz frequency, 12.6 cm wavelength) radar data, Harmon et al. (2011) produced the most complete maps to date of radar reflectivity that indicate the possible locations of water ice at both Mercury poles. These data have been interpreted to show that the PSRs at Mercury's poles may locally contain up to 100 wt% H_2O, with a possible covering of up to 20 cm of dry regolith.

One of the scientific goals of the MErcury Surface, Space ENvironment, GEochemistry, and Ranging (MESSENGER) mission to Mercury (Solomon et al., 2008) is to use planetary neutron spectroscopy to detect and measure hydrogen abundances associated with these polar deposits. The Arecibo radar data, together with Mercury flyby data interrelated with forward models of the response of the MESSENGER Neutron Spectrometer (NS) and spacecraft (Lawrence et al., 2010), allow us for the first time to make specific predictions of the neutron counting rates that will

* Corresponding author.
E-mail address: David.J.Lawrence@jhuapl.edu (D.J. Lawrence).

0032-0633/$ - see front matter © 2011 Elsevier Ltd. All rights reserved.
doi:10.1016/j.pss.2011.07.001

be returned by the NS after MESSENGER is inserted into orbit about Mercury in March 2011. Here we present predicted neutron counting rates for three different scenarios for Mercury polar water ice abundances.

2. Arecibo radar data

Dimensionless radar reflectivity (from Fig. 3b of Harmon et al., 2011) mapped onto 0.125° pixels (expressed as radar cross section per unit surface area) of Mercury's north polar region is shown in Fig. 1a. All signals greater than four standard deviations (4σ) from the noise are regarded as consistent with surface or near-surface expressions of water ice (Harmon et al., 2011).

A number of impact craters contain large areas of enhanced radar reflectivity, as do several intercrater regions. For comparison, the size of the spatial footprint of the NS at full width, half maximum (FWHM) at a spacecraft altitude of 200 km, the lowest periapsis altitude planned for MESSENGER, is illustrated by the dashed white line in Fig. 1a. Because of this large spatial footprint, individual craters will not be resolved with NS data.

Lunar surface temperature data (Paige et al., 2010) show that the Moon's polar cold traps are more extensive than previously thought because they are surrounded by regions in which water ice can be stable at tens of centimeters below the surface. If such near-surface "permafrost" regions are present on Mercury, then the NS signal may be larger than assumed here, since neutron spectroscopy can be sensitive to depths of tens of centimeters (Lawrence et al., 2006).

3. Forward modeling of planetary neutron data

Orbital measurements of epithermal neutrons, having an energy E_n between ~0.4 and ~500 keV, are highly sensitive to the concentration of hydrogen on planetary surfaces (Feldman et al., 1998). The prediction of NS measurements of epithermal neutrons relies on a forward modeling process similar to that used with planetary gamma-ray data (Lawrence et al., 2005; Hagerty et al., 2006). A model distribution of surface hydrogen concentrations at high spatial resolution is derived from available radar data. This abundance distribution is converted to a measurable counting rate map, also at high spatial resolution, using known relations between surface abundances and neutron counting rates. The high-spatial-resolution counting-rate map is converted to a simulated orbital measurement with a known spatial response. Uncertainties from Poisson counting statistics are applied to determine predicted signal-to-background values.

For Mercury, the modeled hydrogen abundance distribution is obtained from the Arecibo radar data. All 0.125° pixels with signals in excess of 4σ are assigned a positive hydrogen concentration (Harmon et al., 2011) and converted to a neutron counting rate associated with a given hydrogen concentration and hydrogen-free soil overburden. We investigate three scenarios: (1) a semi-infinite layer of 100 wt% water ice at the surface in all areas of high radar reflectivity; (2) a semi-infinite layer of 100 wt% water ice covered with 20 cm of dry regolith in all areas of high radar reflectivity; and (3) a semi-infinite layer of 50 wt% water ice

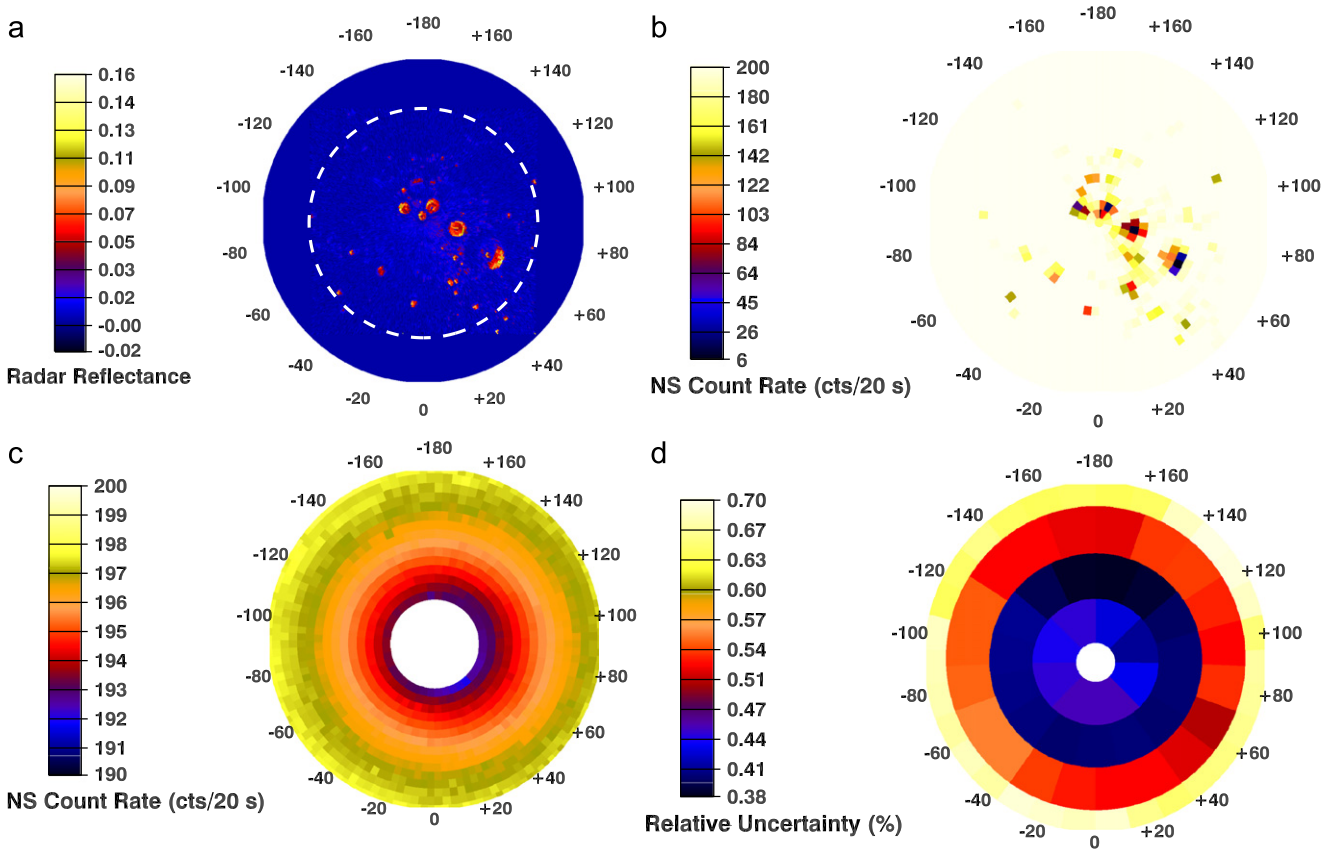

Fig. 1. (a) Mercury radar reflectivity from Harmon et al. (2011), mapped poleward of 80° N at 0.125° per pixel in latitude and longitude. The dashed white line illustrates the size of the NS footprint (at FWHM) for a spacecraft altitude of 200 km. (b) High-spatial-resolution model NS counting rates, poleward of 80° N, binned to 0.5° (~20 km) per pixel under the assumptions that areas of high radar reflectivity have 100 wt% H_2O at the surface and that a fully dry count rate is 200 counts per 20 s. (c) Simulated NS counting rate as propagated through the NS spatial response. This map shows all values poleward of 70° N with no consideration of statistical or systematic uncertainties. (d) Expected uncertainties, poleward of 70° N, from Poisson counting statistics for a one-year MESSENGER primary mission. Pixels are 5° × 5° (~200 km × 200 km).

at the surface in all areas of high radar reflectivity. The first scenario is the large-abundance end-member and has the largest affect on the epithermal neutron signal. This second case is being considered because multiwavelength radar studies suggest that the polar deposits may be covered by 10–20 cm thickness of dry material (Harmon et al., 2011). The third scenario represents a water–ice concentration that is more challenging for detection with orbital neutron measurements.

The MESSENGER NS (Goldsten et al., 2007) has three sensors that make two separate measurements of epithermal neutrons. Two lithium glass (LG) sensors use the spacecraft orientation and velocity relative to Mercury to separate thermal ($E_n < \sim 0.4$ eV) and epithermal ($E_n > \sim 0.4$ eV) neutrons (Feldman and Drake, 1986), where E_n is neutron energy. The NS LG sensor counting rates from the three MESSENGER flybys of Mercury were successfully modeled by Lawrence et al. (2010). The flyby NS measurements were made near Mercury's equator over a region of spectrally intermediate terrain (IT) (Denevi et al., 2009), which we assume here contains no hydrogen because of its high daytime temperatures. We used the best-fit Luna 24-type soil composition determined by Lawrence et al. (2010) for the dry soil portion of the surface material in the three scenarios for the polar deposits investigated here.

The measured net LG neutron counting rate at closest approach (CA) during the flybys was ~10 counts per second (cps). At CA, the spacecraft orientation was characterized by a near-zero value of $\mathbf{V}\bullet\mathbf{x}$, where $\mathbf{V}$ is the spacecraft vector velocity and $\mathbf{x}$ is the spacecraft x-axis unit vector, which is parallel to the normal to one LG detector and anti-parallel to the normal to the other (Lawrence et al., 2010). In this orientation, the two sensors have little sensitivity to thermal neutrons and are mostly sensitive to epithermal neutrons. In orbit, many of the polar measurements of neutron flux will be made at spacecraft attitudes for which at least one of the LG sensors is dominantly sensitive to epithermal neutrons. We therefore use 10 cps as the nominal counting rate for dry Mercury soil, and we assume that at least one sensor will be making measurements of epithermal neutrons during each polar pass. The neutron flux is calculated for the three scenarios, and the validated model of Lawrence et al. (2010) is used to determine the corresponding periapsis counting rates for the $\mathbf{V}\bullet\mathbf{x}=0$ spacecraft orientation. In an ideal situation where polar deposits fill the full NS field of view, the modeled counting rates at 200 km for the three scenarios are 0.034, 0.09, and 0.2 cps. Because we have accurately modeled the NS counting rate (Lawrence et al., 2010), we assume here that we can correct the measured counting rates at different altitudes to a single effective altitude, which we take to be 200 km. Other altitude-dependent effects (e.g., larger statistical uncertainty and larger spatial footprint due to higher altitudes) are treated through the spatial smoothing and uncertainty calculations.

The second epithermal neutron measurement is made by identifying the $^{10}B(n,\alpha)$ reaction in the Gd-wrapped central borated plastic (BP) scintillator (Goldsten et al., 2007) in a manner similar to what was done with a BP scintillator on the Lunar Prospector mission (Genetay et al., 2003; Maurice et al., 2004). Although this sensor provides an independent measure of epithermal neutrons, we are not considering it for this study because its efficiency response has yet to be calculated and validated. Thus, the results here represent a minimum detectability of Mercury hydrogen concentrations, because the BP sensor will provide a second, independent measure of Mercury's polar hydrogen abundances.

From the model counting rates for the first polar deposit scenario, Fig. 1b shows the detected NS counting rates before the spatial resolution of the measurement is included. To simplify later calculations, the 0.125° pixels are rebinned to 0.5° pixels, which are the standard base-map pixels for many planetary nuclear spectroscopy studies (e.g., Lawrence et al., 2004). For hydrogen-rich regions smaller than 0.5° pixels, effective counting rates are determined by the ratio of anhydrous to hydrous deposits in the area containing the hydrogen deposit. The counting rate is given in counts per 20 s, because 20 s is the planned time cadence for NS measurements from the Mercury orbit.

The spatial resolution of the NS is simulated using spatial response functions for planetary nuclear spectroscopy (Lawrence et al., 2003; Maurice et al., 2004). The FWHM of the spatial response is linearly dependent on spacecraft altitude and scales as approximately as 1.5× altitude. Because of MESSENGER's highly eccentric, near-polar orbit (200 km periapsis altitude to 15,000 km apoapsis altitude, and 82.5–84° inclination) (Leary et al., 2007), the effective NS spatial resolution is highly variable and generally dependent on latitude. Previous equal-area algorithms for calculating the spatial resolution were for a near-constant altitude (Lawrence et al., 2004), so a new altitude-dependent code for equal-area, spherical smoothing was implemented to account for the large altitude variations in MESSENGER's elliptical orbit.

4. Results and discussion

The result of smoothing the count rate map of Fig. 1b is shown in Fig. 1c. This map represents a best-case LG measurement with no consideration of statistical or systematic uncertainties. The circular gap centered on the pole reflects the fact that MESSENGER's orbital inclination is planned not to exceed 85°, so there will be no sub-spacecraft measurements poleward of this latitude. Although no individual craters are resolved, the model hydrogen distribution creates a signal that is 4.1% lower than the count rate for dry material. For comparison, the maximum signal magnitudes for cases 2 and 3 are 3.9% and 3.4% below that for dry soil, respectively. For reference, this magnitude of the signal is about two-thirds that measured for Cabaeus crater near the lunar south pole by the Lunar Prospector Neutron Spectrometer (Feldman et al., 2001).

The extent to which these signals can be detected depends critically on the expected measurement uncertainties. Fig. 1d shows the lower-limit uncertainties from Poisson counting statistics, now mapped onto 200×200 km^2 quasi-equal-area pixels, where the maximum collection time per pixel is ~10,000 s. These uncertainties are for a one-year MESSENGER primary mission, an 85% duty cycle, and altitude-dependent corrections to the total counts so that the count rate uncertainties are properly calculated. With no other systematic uncertainties, signal-to-background detections of 11σ, 10σ, and 9σ can be achieved on 200×200 km^2 pixels for each of the three cases. In principle, detections with higher significance could be made for longitudinally averaged data. If the uncertainties are sufficiently low, longitudinal variations reflecting the longitudinal asymmetry of the hydrogen distribution could also be detected. However, given the highly asymmetric orbit and the models that are required to correct the systematic variations in the neutron data (Lawrence et al., 2010), as well as previous analyses of planetary neutron data (e.g., Maurice et al., 2004), we expect that the overall systematic uncertainties will be no better than 0.5–1%. In such a case, detections of 4–8σ signals are achievable.

We again note that these predictions are made for only the NS LG sensors and do not include independent measurements from the NS BP sensor, which made clear detections of epithermal neutrons at Mercury (Fig. 2). Fig. 3 shows the net BP epithermal neutron count rate versus time during MESSENGER's first Mercury flyby. The net CA counting rate of ~35 cps is more than a factor of three larger than the LG CA net counting rate of

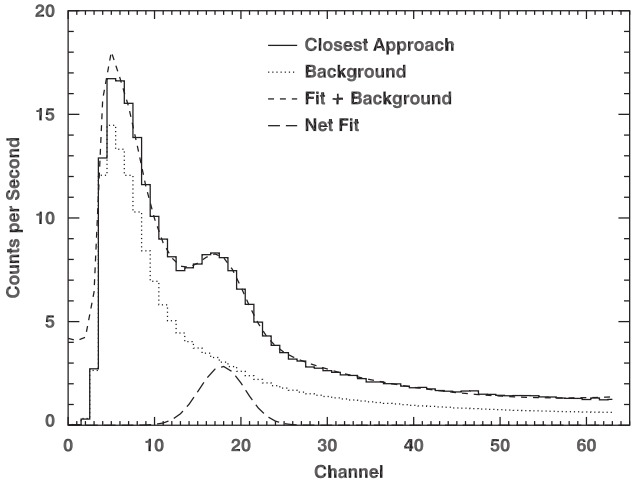

Fig. 2. BP singles pulse height data from MESSENGER's first Mercury flyby on 14 January 2008. Pulse height data taken ± 10 min around closest approach (CA) are shown by the solid black line. The peak at channel 17 is the $^{10}B(n,\alpha)$ reaction indicating epithermal neutron detections. Mean background counts from before and after CA are shown by the dotted line. A fit to a scaled background and the $^{10}B(n,\alpha)$ peak is shown as a short dashed line. The peak after the background has been subtracted is shown as the long dashed line.

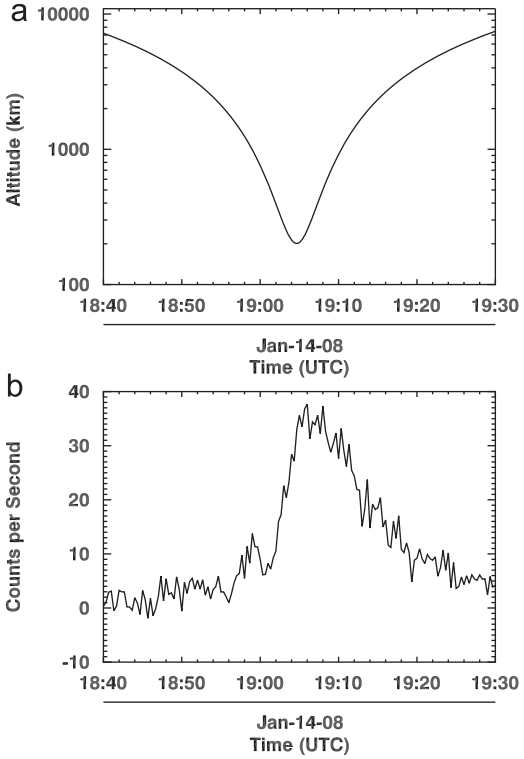

Fig. 3. NS data from MESSENGER's first Mercury flyby on 14 January 2008 (Lawrence et al., 2010). (a) Altitude versus time during the flyby. The altitude at closest approach was 200 km. (b) Net borated plastic singles count rate vs. time.

$\sim$10 cps. Thus, if the systematic uncertainties can be sufficiently reduced, the statistical precision of the BP data could be almost a factor of two better than that of the LG data.

5. Conclusions

From Earth-based radar images of Mercury and MESSENGER NS data from the Mercury flybys, we have calculated the predicted neutron counting rates and uncertainties for Mercury's north polar region at the end of MESSENGER's one-year prime mission at Mercury. Because of the large spatial footprint of the NS measurements, the polar deposits within individual craters will not be resolvable with the NS data. However, if hydrogen abundances are sufficiently large, as is suggested by the Earth-based radar data, then statistically significant hydrogen signals should be detected by NS LG data. The ability to make statistically significant polar hydrogen measurements is strengthened by epithermal neutron measurements with the NS BP sensor, which has a CA counting rate a factor of $\sim$3.5 times larger than the LG sensors. After one year of orbital data collection, the MESSENGER NS should therefore enable substantial progress to be made in our understanding of the nature of Mercury's polar deposits. If these deposits have large concentrations of hydrogen, then such high concentrations should be confirmed by the NS measurements. If the polar deposits are not enriched with hydrogen, but are dominated by other elements, e.g., sulfur (Sprague et al., 1995), then the MESSENGER neutron measurements should be able to place robust lower limits on the hydrogen concentrations near Mercury's north pole and may also be able to detect large concentrations of sulfur ($\sim$80 wt%) through decreases in the flux of thermal neutrons (Feldman et al., 1997).

Acknowledgments

The authors thank Lucy Lim and an anonymous reviewer for helpful comments of this paper. The work on this study was supported in part by the MESSENGER Participating Scientist Program. The MESSENGER project is supported by the NASA Discovery Program under contracts NASW-00002 to the Carnegie Institution of Washington and NAS5-97271 to the Johns Hopkins University Applied Physics Laboratory.

References

Arnold, J.R., 1979. Ice in the lunar polar regions. J. Geophys. Res. 84, 5659–5668.
Denevi, B.W., Robinson, M.S., Solomon, S.C., Murchie, S.L., Blewett, D.T., Domingue, D.L., McCoy, T.J., Ernst, C.M., Head, J.W., Watters, T.R., Chabot, N.L., 2009. The evolution of Mercury's crust: a global perspective from MESSENGER. Science 324, 613–619.
Feldman, W.C., Drake, D.M., 1986. A Doppler filter technique to measure the hydrogen content of planetary surfaces. Nucl. Instrum. Methods, Sect. A 245, 182–190.
Feldman, W.C., Barraclough, B.L., Hansen, C.J., Sprague, A.L., 1997. The neutron signature of Mercury's volatile polar deposits. J. Geophys. Res. 102, 25565–25574.
Feldman, W.C., Maurice, S., Binder, A.B., Barraclough, B.L., Elphic, R.C., Lawrence, D.J., 1998. Fluxes of fast and epithermal neutrons from Lunar Prospector: evidence for water ice at the lunar poles. Science 281, 1496–1500.
Feldman, W.C., Maurice, S., Lawrence, D.J., Little, R.C., Lawson, S.L., Gasnault, O., Wiens, R.C., Barraclough, B.L., Elphic, R.C., Prettyman, T.H., Steinberg, J.T., Binder, A.B., 2001. Evidence for water ice near the lunar poles. J. Geophys. Res. 106 (E10), 23231–23252.
Genetay, I., Maurice, S., Feldman, W.C., Gasnault, O., Lawrence, D.J., Elphic, R.C., d'Uston, L., Binder, A.B., 2003. Elemental content from 0 to 500 keV neutrons: Lunar Prospector results. Planet. Space Sci. 51, 271–280.
Goldsten, J.O., Rhodes, D.A., Boynton, W.V., Feldman, W.C., Lawrence, D.J., Trombka, J.I., Smith, D.M., Evans, L.G., White, J., Madden, N.W., Berg, P.C., Murphy, G.A., Gurnee, R.S., Strohbehn, K., Williams, B.D., Schaefer, E.D., Monaco, C.A., Cork, C.P., Eckels, J.E., Miller, W.O., Burks, M.T., Hagler, L.B., Deteresa, S.J., Witte, M.C., 2007. The MESSENGER Gamma-Ray and Neutron Spectrometer. Space Sci. Rev. 131, 339–391.
Hagerty, J.J., Lawrence, D.J., Hawke, B.R., Vaniman, D.T., Elphic, R.C., Feldman, W.C., 2006. Refined thorium abundances for lunar red spots: implications for evolved, non-mare volcanism on the Moon. J. Geophys. Res. 111, E06002. doi:10.1029/2005JE002592.
Harmon, J.K., Slade, M.A., 1992. Radar mapping of Mercury: full-disk images and polar anomalies. Science 258, 640–643.
Harmon, J.K., Slade, M.A., Rice, M.S., 2011. Radar imagery of Mercury's putative polar ice: 1999–2005 Arecibo results. Icarus 211, 37–50. doi:10.1016/j.icarus,2010.08.007.

Lawrence, D.J., Elphic, R.C., Feldman, W.C., Prettyman, T.H., Gasnault, O., Maurice, S., 2003. Small-area thorium features on the lunar surface. J. Geophys. Res. 108 (E9), 5102. doi:10.1029/2003JE002050.

Lawrence, D.J., Maurice, S., Feldman, W.C., 2004. Gamma-ray measurements from Lunar Prospector: time series data reduction for the Gamma-Ray Spectrometer. J. Geophys. Res. 109, E07S05. doi:10.1029/2003JE002206.

Lawrence, D.J., Hawke, B.R., Hagerty, J.J., Elphic, R.C., Feldman, W.C., Prettyman, T.H., Vaniman, D.T., 2005. Evidence for a high-Th, evolved lithology on the Moon at Hansteen Alpha. Geophys. Res. Lett. 32, L07201. doi:10.1029/2004GL022022.

Lawrence, D.J., Feldman, W.C., Elphic, R.C., Hagerty, J.J., Maurice, S., McKinney, G.W., Prettyman, T.H., 2006. Improved modeling of Lunar Prospector neutron spectrometer data: implications for hydrogen deposits at the lunar poles. J. Geophys. Res. 111, E08001. doi:10.1029/2005JE002637.

Lawrence, D.J., Feldman, W.C., Goldsten, J.O., McCoy, T.J., Blewett, D.T., Boynton, W.V., Evans, L.G., Nittler, L.R., Rhodes, E.A., Solomon, S.C., 2010. Identification and measurement of neutron-absorbing elements on Mercury's surface. Icarus 209, 195–209. doi:10.1016/j.icarus.2010.04.005.

Leary, J.C., Conde, R.F., Dakermanji, G., Engelbrecht, C.S., Ercol, C.J., Fielhauer, K.B., Grant, D.G., Hartka, T.J., Hill, T.A., Jaskulek, S.E., Mirantes, M.A., Mosher, L.E., Paul, M.V., Persons, D.F., Rodberg, E.H., Srinivasan, D.K., Vaughan, R.M., Wiley, S.R., 2007. The MESSENGER spacecraft. Space Sci. Rev. 131, 187–217.

Lucey, P.G., 2009. The poles of the Moon. Elements 5, 41–46. doi:10.2113/gselements.5.1.41.

Maurice, S., Lawrence, D.J., Feldman, W.C., Elphic, R.C., Gasnault, O., 2004. Reduction of neutron data from Lunar Prospector. J. Geophys. Res. 109, E07S04. doi:10.1029/2003JE002208.

Paige, D.A., Wood, S.E., Vasavada, A.R., 1992. The thermal stability of water ice at the poles of Mercury. Science 258, 643–646.

Paige, D.A., Siegler, M.A., Zhang, J.A., Hayne, P.O., Foote, E.J., Bennett, K.A., Vasavada, A.R., Greenhagen, B.T., Schofield, J.T., McCleese, D.J., Foote, M.C., DeJong, E., Bills, B.G., Hartford, W., Murray, B.C., Allen, C.C., Snook, K., Soderblom, L.A., Calcutt, S., Taylor, F.W., Bowles, N.E., Bandfield, J.L., Elphic, R., Ghent, R., Glotch, T.D., Wyatt, M.B., Lucey, P.G., 2010. Diviner Lunar Radiometer observations of cold traps in the Moon's south polar region. Science 330, 479–482.

Slade, M.A., Butler, B.J., Muhleman, D.O., 1992. Mercury radar imaging: evidence for polar ice. Science 258, 635–640.

Solomon, S.C., McNutt Jr., R.L., Watters, T.R., Lawrence, D.J., Feldman, W.C., Head, J.W., Krimigis, S.M., Murchie, S.L., Phillips, R.J., Slavin, J.A., Zuber, M.T., 2008. Return to Mercury: a global perspective on MESSENGER's first Mercury flyby. Science 321, 59–62.

Sprague, A.L., Hunten, D.M., Lodders, K., 1995. Sulfur at Mercury, elemental at the poles and sulfides in the regolith. Icarus 118, 211–215.

Vasavada, A.R., Paige, D.A., Wood, S.E., 1999. Near-surface temperatures on Mercury and the Moon and the stability of polar ice deposits. Icarus 141, 179–193.

Watson, K., Murray, B.C., Brown, H., 1961. The behavior of volatiles on the lunar surface. J. Geophys. Res. 66, 3033–3045.